J Electroceram (2006) 16:229–238
DOI 10.1007/s10832-006-8278-9

Theoretical analysis of the impedance spectra of electroceramics Part 2: isotropic grain boundaries

R. Bouchet · P. Knauth · J.-M. Laugier

Received: 3 May 2005 / Revised: 25 January 2006 / Accepted: 13 March 2006

Abstract The grain-size dependence of impedance spectra of electroceramics is simulated, based on a brick layer model with explicit consideration of parallel boundaries. A constant grain interior conductivity is assumed and the grain boundary (gb) conductivity is varied. Parallel and series gb are assumed isotropic, i.e. charge transport along and across gb is supposed identical. Various grain sizes between 500 and 0.5 nm are studied and impedance spectra are shown in complex plane and Bode representations.

Keywords Nanocomposite · Nanoceramics · Grain boundaries · Impedance spectroscopy

1. Introduction

Boundaries play a very important role for the electrical properties of polycrystalline (ceramic) and polyphase (composite) materials. A boundary can be defined as a two-dimensional transition region between two phases (then more precisely: phase boundary) or two grains (then more precisely: grain boundary, gb). In the following, the term "interface" is used as synonym of the word "boundary". To understand their influence, it is necessary to consider transport along (i.e. parallel to) the boundary and transport across (i.e. perpendicular to) the boundary. The problem of transport along and across interfaces in polycrystalline ionic conductors has been tackled by Jamnik and Maier [1].

A gb can be represented by a core region, with modified defect concentrations and mobilities, and two adjacent and symmetrical space charge regions with modified charge carrier concentrations, but carrier mobilities identical to the grain interior values, according to the space charge model [2]. One has also to take explicitly into account the type of electrical conduction in the considered material. In electronically conducting solids, a generally accepted physical interpretation for charge carrier blocking at boundaries is the presence of interface states due to segregated impurities or defects, which "trap" the electronic carriers. The associated depletion regions around the boundary can be described as double Schottky barriers [3].

In solid ionic conductors, "parallel" boundaries can provide fast conduction paths for ions. It is well known for a long time in metallic materials that the high defect density and large free volume in the boundary core lead to enhanced atomic transport so that the boundary core represents a high diffusivity region. This enhanced intergranular diffusion was also observed in ionic solids, such as oxides [4]. A blocking character of perpendicular boundaries (in the following also called "series" boundaries) is often interpreted by the presence at the boundary core of a precipitated secondary phase with low conductivity, leading to current constriction effects [5]. A conceptual difficulty is that high conductivity parallel boundaries must percolate through the whole sample in order to give a measurable enhancement effect, which means that the ionic charge carriers must also pass perpendicular boundaries. This problem can however be lifted by considering that the perpendicular gb are inhomogeneous, so that the charge carriers can "leak" through.

The importance of highly conducting space charge regions adjacent to the boundary core for conductivity enhancement and blocking effects has been demonstrated in ionic conductor composites and thin-films [2]. Enhancement effects are expected if accumulation layers with increased charge carrier concentration are formed. Depletion layers lead to charge carrier blocking effects. Boundary blocking due to

R. Bouchet (✉) · P. Knauth · J.-M. Laugier
Madirel (UMR 6121), Université de Provence-CNRS,
Centre St Jérôme, 13397 Marseille Cedex 20, France
e-mail: renaud.bouchet@up.univ-mrs.fr

ionic charge carrier depletion in space charge zones was discussed recently in zirconia [6]. These effects can be treated by analytical equations in the semi-infinite case or by numerical simulations when grain size and Debye length become comparable (mesoscopic effects) [7].

A very elegant experimental method to study transport in the grain interior ("bulk") and at interfaces is impedance spectroscopy, i.e. measurements of the a.c. current response to a small a.c. voltage perturbation (or vice versa) as function of the a.c. frequency. The characteristic time constants of bulk and boundary responses are given by the ratio of specific electrical properties, i.e. dielectric permittivity over electrical conductivity. The grain interior contribution is usually observed at high frequency, whereas the contribution of series gb is observed at lower frequency. Since the classical work of Bauerle in 1969 [8], the electrical properties of polycrystalline materials are generally determined by this technique with a.c. frequencies typically in the range between 10^6 and 10^{-1} s^{-1} [9]. However, one has to assume an equivalent circuit representing the 3D sample topology of polycrystalline or polyphase materials in order to interpret raw impedance data.

Still the most important approach is the elementary bricklayer model (BLM) outlined at the end of the 1970's [10–12]. In this model, the grains are represented by cubes with a certain size, separated by homogeneous gb with constant thickness (in our case: 0.5 nm, which is the value adopted in the classical Fisher model of gb diffusion [13]). Finite element calculations in microcrystalline ceramics considered deviations from cubic grain shape, a grain size distribution, imperfect contact between grains, due to pores or secondary phases, and inhomogeneous gb with a conductivity distribution [14–16]. For polycrystalline materials with sufficiently large grain size, the contribution of "parallel" boundaries to the current transport is generally negligible, given the very unfavorable ratio of grain and parallel boundary areas.

However, the contribution of parallel boundaries increases with decreasing grain size and if the parallel gb conductivity is significantly larger than the grain conductivity [17]. An impedance analysis of polycrystalline ceramics based on a "generalized" BLM with resistive grain boundaries was presented by Mason and coworkers [18, 19]. Very recently, a 3D composite model was developed for polycrystalline materials covering grain boundary volume fractions from near 1 (nanoscale) to near 0 (microscale) [20] and including grain shape and periodicity effects [21]. In the limit of nanocrystalline materials, where grain size and gb width become comparable, the parallel path can have a significant influence on the overall impedance of the sample. Kleinlogel and Gauckler [22] studied the case of CoO-CeO_2 nanocomposites and showed the influence of the parallel boundaries on the electrical properties: a change from ionic to electronic conduction can be observed depending on the experimental conditions. Furthermore, they used impedance spectroscopy to analyze the sample microstructure.

We have generalized the BLM analysis, taking parallel gb path explicitly into account and calculating analytical equations for one unit cell and for a 3-dimensional model ceramic [23]. In this work, we assumed a strongly anisotropic behavior of the boundaries, in accordance with the usual assumption in the electroceramics community. The conductivity along the parallel boundary ("parallel" conductivity) was varied between very small and very large values. The conductivity across the series boundary ("perpendicular" conductivity) was taken as a small constant value, in other words the series boundary was considered blocking. The dielectric permittivity was assumed identical for grain interior and boundaries. The numerical simulation for constant gb thickness (0.5 nm) and three grain sizes (5, 50, 500 nm) showed that below a certain threshold value of parallel conductivity, depending on the grain size, the influence of the parallel path is negligible. Above this value however, the influence of the parallel path can lead to significant errors and, at the smallest nanocrystalline size, totally wrong conclusions can be drawn using the classical BLM.

The following results were derived in this case:

1) An important conclusion is that grain and gb arcs do not overlap with decreasing grain size in the complex plane representation. Two impedance arcs are always observed, except if the ratio dielectric permittivity over electrical conductivity is identical for grain and gb.
2) A simple criterion for the validity of the classical BLM is based on the characteristic relaxation frequencies for low and high frequency arcs. As long as they are grain-size independent, the influence of the parallel path is negligible and the BLM can be used. For large grain sizes, this is usually the case.
3) If the relaxation frequencies change, the usual attribution of low frequency response to blocking gb and high frequency arc to grain interior is incorrect. The observed impedance is a complex combination of the electrical parameters of the different elements, which must then be calculated by resolution of the complicated analytical equations.

However, our previous approach did not take into account the following points:

1) The anisotropic case was discussed, but the "isotropic" case, where parallel and perpendicular gb conductivity are identical, was not considered.
2) Further size reduction below 5 nm leads to a case, where grain and gb regions have comparable size, but different conductivity. The grain size variation discussed here leads all the way from a single crystal to a material with

sub-nanometer domains with different conductivity, which can be assimilated to a "core-shell" nanocomposite solid.

In the following, we present an extension of our previous approach.

2. Theoretical analysis

Figure 1 shows a schematic representation of a polycrystalline material used in the BLM and below one unit cube, representing an individual grain with grain size D and its 6 boundaries (thickness d) with adjacent grains. The equivalent electrical circuit is shown in Fig. 2.

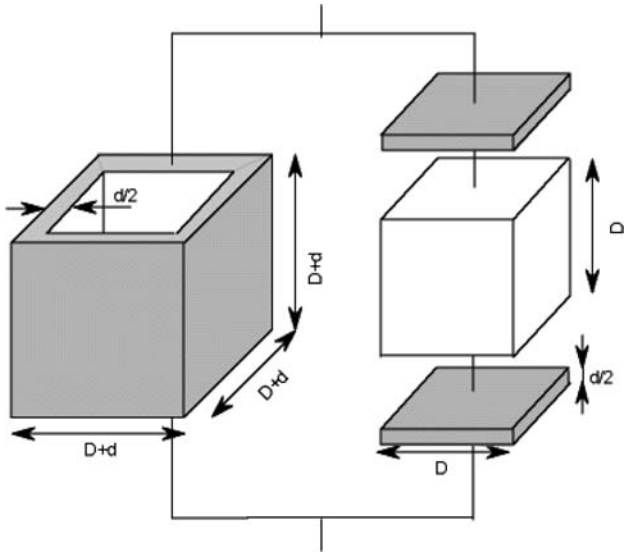

Fig. 1 (a) Brick layer model and (b) one unit cube.

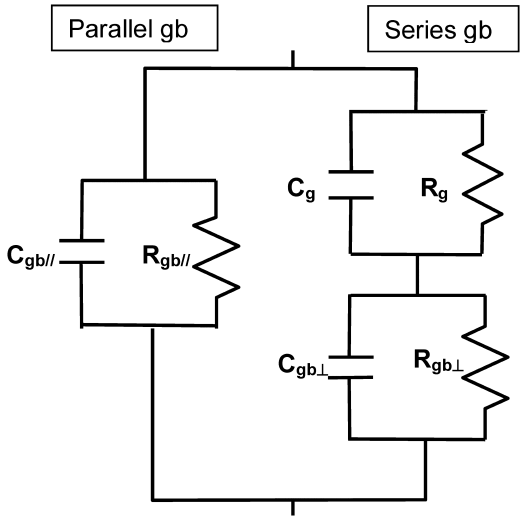

Fig. 2 (a) Electrical equivalent circuit.

The grain volume equals D^3 and its electrical properties are the electrical conductivity σ_g and the dielectric permittivity ε_g. The volume of the parallel gb can be written:

$$V_{gb//} = (2D + d)(D + d)d \tag{1}$$

The volume of the series gb is:

$$V_{gb\perp} = D^2 d \tag{2}$$

The electrical conductivity σ_{gb} and the dielectric permittivity ε_{gb} are assumed identical for parallel and series gb ($\sigma_{gb\perp} = \sigma_{gb//} = \sigma_{gb}$).

2.1. Series path of the equivalent circuit for one unit cube

On the series side, the resistance and capacitance of grain and (perpendicular) gb can be written (cf. Fig. 2):

$$\begin{cases} R_g = \dfrac{1}{\sigma_g D} & (3) \\ C_g = \varepsilon_g D & (4) \end{cases}$$

$$\begin{cases} R_{gb\perp} = \dfrac{d}{\sigma_{gb} D^2} & (5) \\ C_{gb\perp} = \dfrac{\varepsilon_{gb} D^2}{d} & (6) \end{cases}$$

The grain impedance equals (j: imaginary unit):

$$Z_g = \frac{R_g}{1 + j\omega R_g C_g} \tag{7}$$

The characteristic circular frequency of relaxation is:

$$\omega_g = \frac{1}{R_g C_g} = \frac{\sigma_g}{\varepsilon_g}. \tag{8}$$

One can write similar equations for the series gb:

$$Z_{gb\perp} = \frac{R_{gb\perp}}{1 + j\omega R_{gb\perp} C_{gb\perp}} \tag{9}$$

The characteristic circular frequency of the series gb is:

$$\omega_{gb} = \frac{\sigma_{gb}}{\varepsilon_{gb}} \tag{10}$$

2.2. Parallel path of the equivalent circuit for one unit cube

The resistance and capacitance of parallel gb are:

$$R_{gb//} = \frac{D + d}{\sigma_{gb}(2D + d)d} \tag{11}$$

$$C_{gb//} = \frac{\varepsilon_{gb}(2D + d)d}{(D + d)} \tag{12}$$

The impedance of the parallel gb is:

$$Z_{gb//} = \frac{R_{gb//}}{1 + j\omega R_{gb//}C_{gb//}} \tag{13}$$

The characteristic circular frequency of the parallel gb is:

$$\omega_{gb//} = \frac{\sigma_{gb}}{\varepsilon_{gb}} \tag{14}$$

2.3. Total equivalent circuit for one unit cube

The total impedance is given by the equation:

$$Z = \frac{(Z_g + Z_{gb\perp})Z_{gb//}}{Z_g + Z_{gb\perp} + Z_{gb//}} \tag{15}$$

After some elementary (but time-consuming) algebra, the final Eq. (16) follows:

$$Z = \frac{\dfrac{R_{gb//}(R_g + R_{gb\perp})}{R_g + R_{gb\perp} + R_{gb//}}\left[1 + j\omega\dfrac{R_gR_{gb\perp}(C_g + C_{gb\perp})}{R_g + R_{gb\perp}}\right]}{1 + j\omega\dfrac{[R_gC_g(R_{gb\perp} + R_{gb//}) + R_{gb\perp}C_{gb\perp}(R_g + R_{gb//}) + R_{gb//}C_{gb//}(R_g + R_{gb\perp})]}{R_g + R_{gb\perp} + R_{gb//}} - \omega^2\dfrac{R_gR_{gb\perp}R_{gb//}(C_gC_{gb\perp} + C_gC_{gb//} + C_{gb\perp}C_{gb//})}{R_g + R_{gb\perp} + R_{gb//}}} \tag{16}$$

This equation is of the form:

$$Z = \frac{K(1 + j\omega\tau_1)}{1 + j\omega\tau_2 + (j\omega\tau_3)^2} \tag{17}$$

It is analogue to that obtained for a classical circuit composed of two parallel resistor-capacitor elements in series $\{(R_1//C_1)\perp(R_2//C_2)\}$. In other words, the two circuits $\{(R_1//C_1)\perp(R_2//C_2)\}$ and $\{(R_{gb////}C_{gb//})//[(R_g//C_g)\perp(R_{gb\perp}//C_{gb\perp})]\}$ have a similar impedance response. The relations between the two circuits can be obtained by solving a system of 4 equations with 4 unknown (R_1, R_2, C_1, C_2) and 6 relevant parameters ($R_{gb//}$, $C_{gb//}$, R_g, C_g, $R_{gb\perp}$, $C_{gb\perp}$), including the equation:

$$R_1 + R_2 = \frac{R_{gb//}(R_g + R_{gb\perp})}{(R_g + R_{gb\perp} + R_{gb//})} \tag{18}$$

There is no unique solution of this set of equations, but several parameter sets can solve this system. This means that at least 2 of the 6 parameters must be known in order to determine the others. The algebraic resolution gives non-linear and very clumsy results [23]. One of the main conclusions is that whatever the effect of the parallel path, one observes two arcs in the complex plane "Nyquist" plot if the relaxation frequency of grain and series gb are different ($\nu_g \neq \nu_{gb}$) and one arc only in the case $\nu_g \approx \nu_{gb}$. This means also that grain and gb arcs do not overlap with decreasing grain size, but only if the specific electrical properties become equal. For small differences of the characteristic circular frequencies, it is more appropriate to show the impedance data in the Bode representation, i.e. as function of a.c. frequency.

2.4. Impedance of a 3-dimensional (3D) sample

To extent the calculation from one unit cube to a 3D ceramics, we introduce the number N_L of grains and series gb in a 3D sample of thickness L:

$$N_L = L/(D + d) \tag{19}$$

Furthermore, we calculate the number of grains and gb per unit area using the surface area of the 3D sample of radius r:

$$N_S = \pi r^2/(D + d)^2 \tag{20}$$

We have N_L grains in series forming a transmission line. N_S of these transmission lines are in parallel. An elementary calculation gives the total impedance Z_{tot} of the 3D ceramics, using Eq. (15):

$$Z_{tot} = \frac{L}{\pi r^2}(D + d)\frac{Z_{gb//}(Z_g + Z_{gb\perp})}{Z_{gb//} + Z_{gb\perp} + Z_g} \tag{21}$$

2.5. Numerical simulation

Impedance spectra are simulated for a cylindrical sample of 4 mm diameter and 1 mm thickness. The grain size effect is observed for grain sizes between 500 and 0.5 nm. In all simulations, the gb thickness is assumed to be $d = 0.5$ nm, the value adopted in the classical Fisher model of gb diffusion. The dielectric permittivities are set equal, assuming a typical dielectric constant of 10. The grain conductivity is taken as 10^{-3} S/m and the gb conductivity is varied between 10^{-7} and 1 S/m. The a.c. frequency is varied between 10^8 and 10^{-3} s^{-1}. The Figs. 3a–6a present normalized complex plane impedance spectra using the BLM model for 4 discrete grain size values: 500, 50, 5 and 0.5 nm. Impedance data in Bode representation are shown in Fig. 3b–6b (modulus) and 3c–6c (phase). The influence of the gb conductivity on the impedance at low frequency is here observed more easily than in the complex plane plots. Furthermore, we show in Figure 7a grain size dependence of the ceramic electrical conductivity, calculated using the BLM.

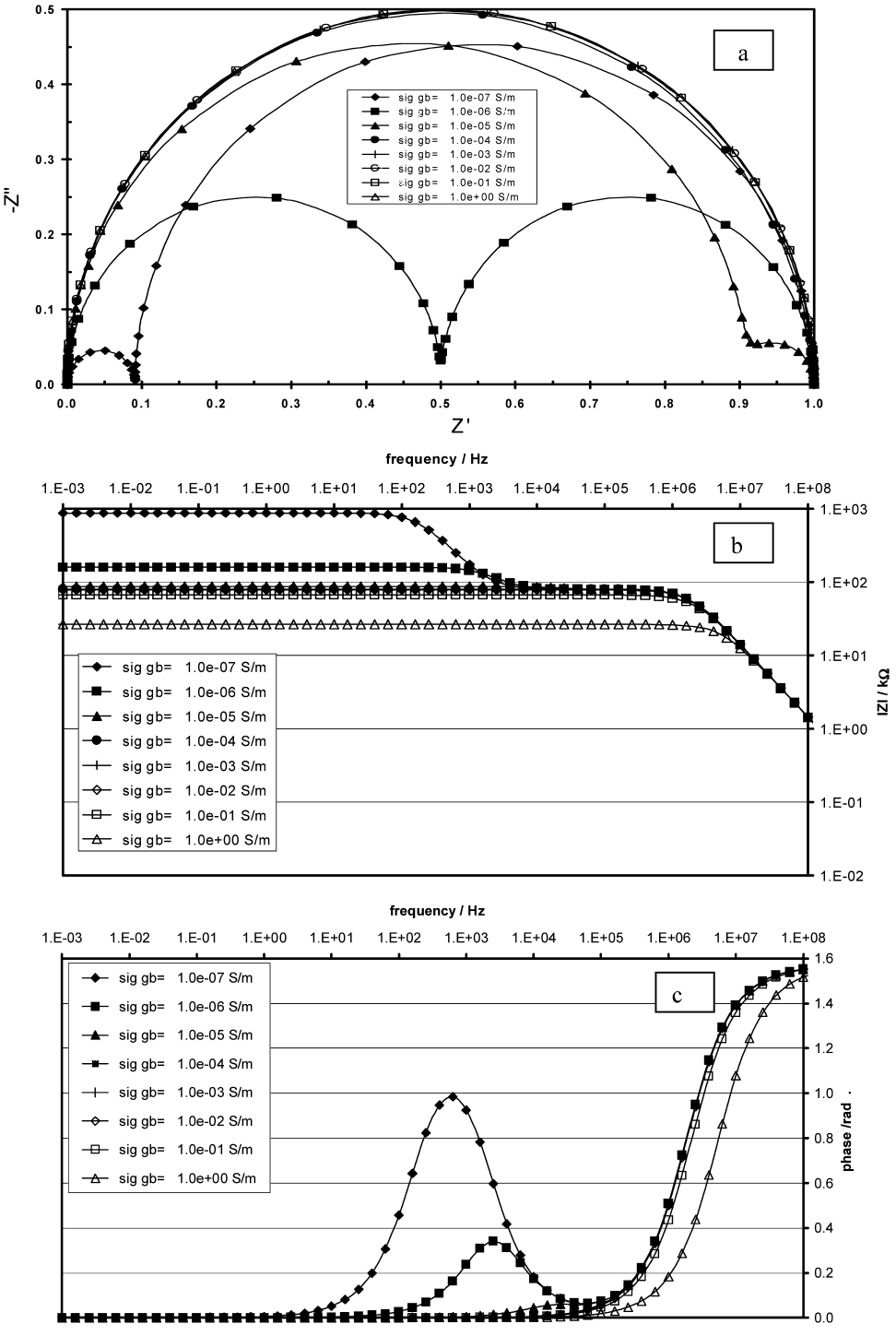

Fig. 3 Simulated impedance spectra for a cylindrical pellet with 4 mm diameter and 1 mm thickness. The mean grain size is taken as $D = 500$ nm. The grain conductivity is taken as $\sigma_g = 10^{-3}$ S/m and the gb conductivity is varied between 10^{-7} and 1 S/m. a) Complex plane plot, b) Bode modulus representation, c) Bode phase representation.

3. Results and discussion

The main features of this model can be discussed for two ceramic microstructures with extreme grain sizes. For the largest grain size (500 nm, Fig. 3), the respective contribution of grain and gb to the overall resistance can be estimated easily for low gb conductivity $\sigma_{gb} \leq 10^{-5}$ S/m from the complex plane plot (Fig. 3a, see below Eq. (26)). In the Bode representations (Fig. 3b and c), two time constants can be clearly observed, the resistance of the series gb is observed at low frequency, and the bulk resistance is not changed. For higher grain boundary conductivity values, only one relaxation time is visible in the investigated frequency range. For a gb conductivity above the grain value ($\sigma_{gb} > 10^{-3}$ S/m), the analytical equations must in principle be resolved to calculate the different electrical parameters. However, given the

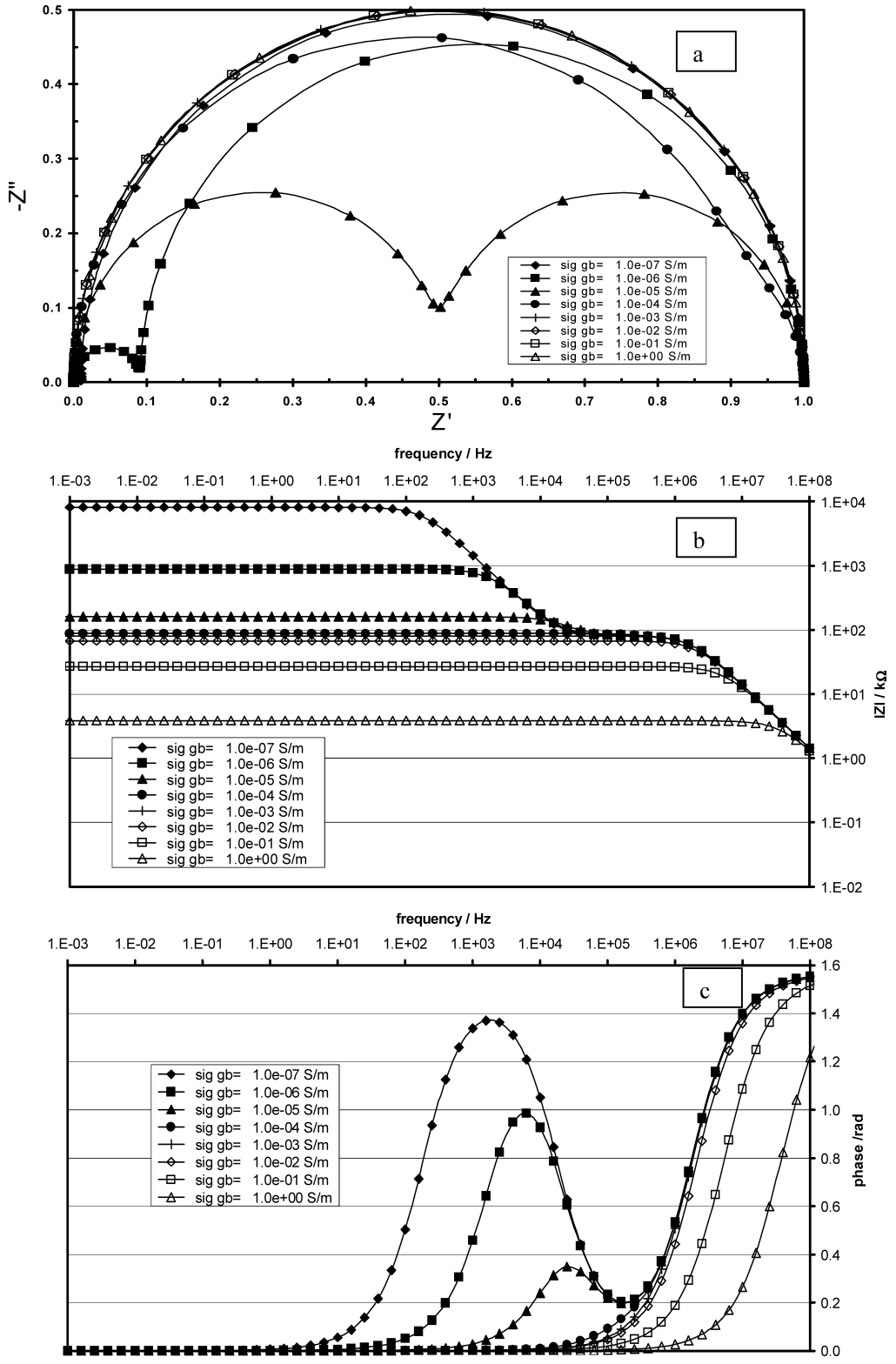

Fig. 4 Simulated impedance spectra using the BLM model for a cylindrical pellet with 4 mm diameter and 1 mm thickness. The mean grain size is taken as $D = 50$ nm. The grain conductivity is taken as $\sigma_g = 10^{-3}$ S/m and the gb conductivity is varied between 10^{-7} and 1 S/m. a) Complex plane plot, b) Bode modulus representation, c) Bode phase representation.

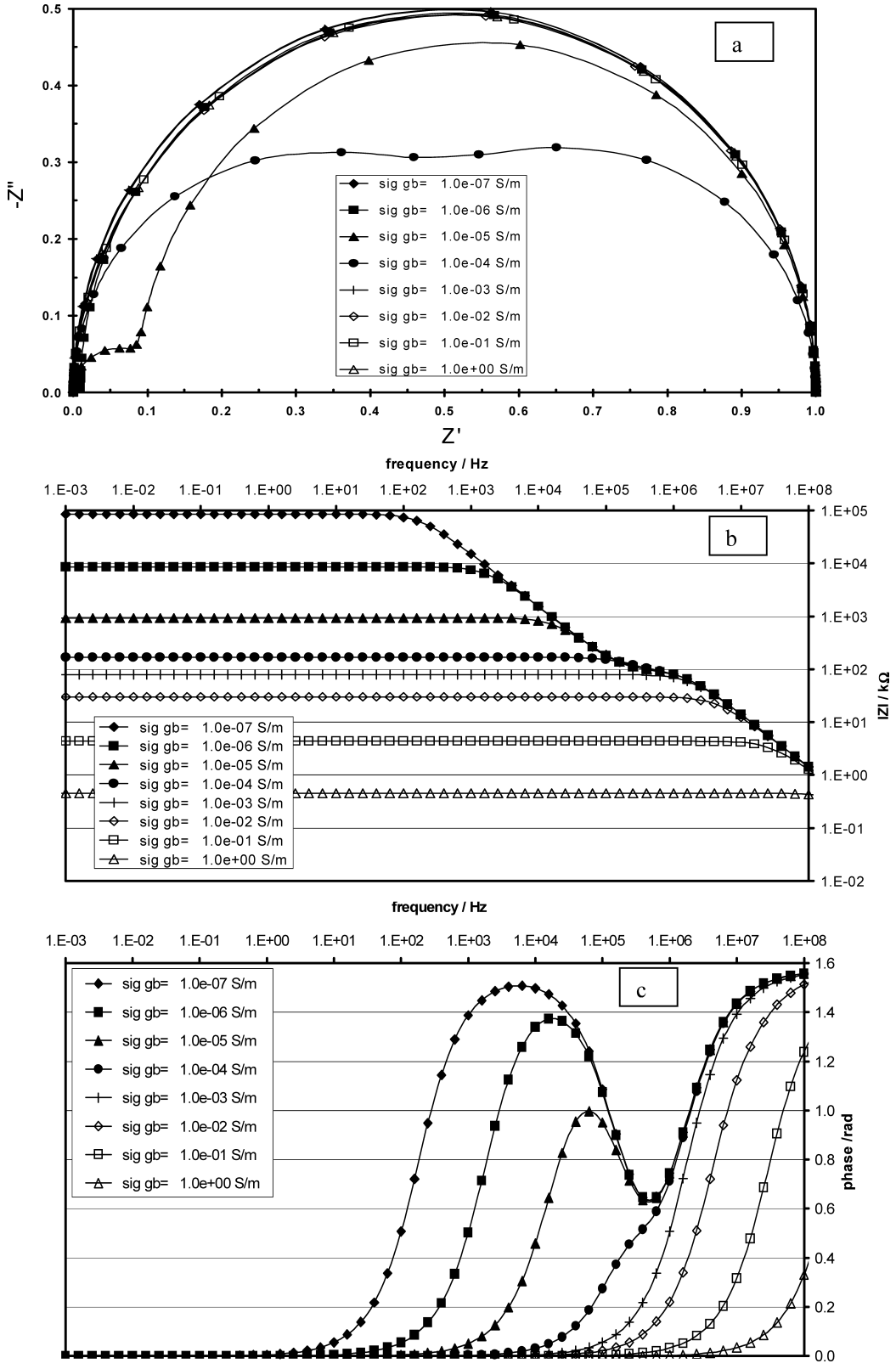

Fig. 5 Simulated impedance spectra using the BLM model for a cylindrical pellet with 4 mm diameter and 1 mm thickness. The mean grain size is taken as $D = 5$ nm. The grain conductivity is taken as $\sigma_g = 10^{-3}$ S/m and the gb conductivity is varied between 10^{-7} and 1 S/m. a) Complex plane plot, b) Bode modulus representation, c) Bode phase representation.

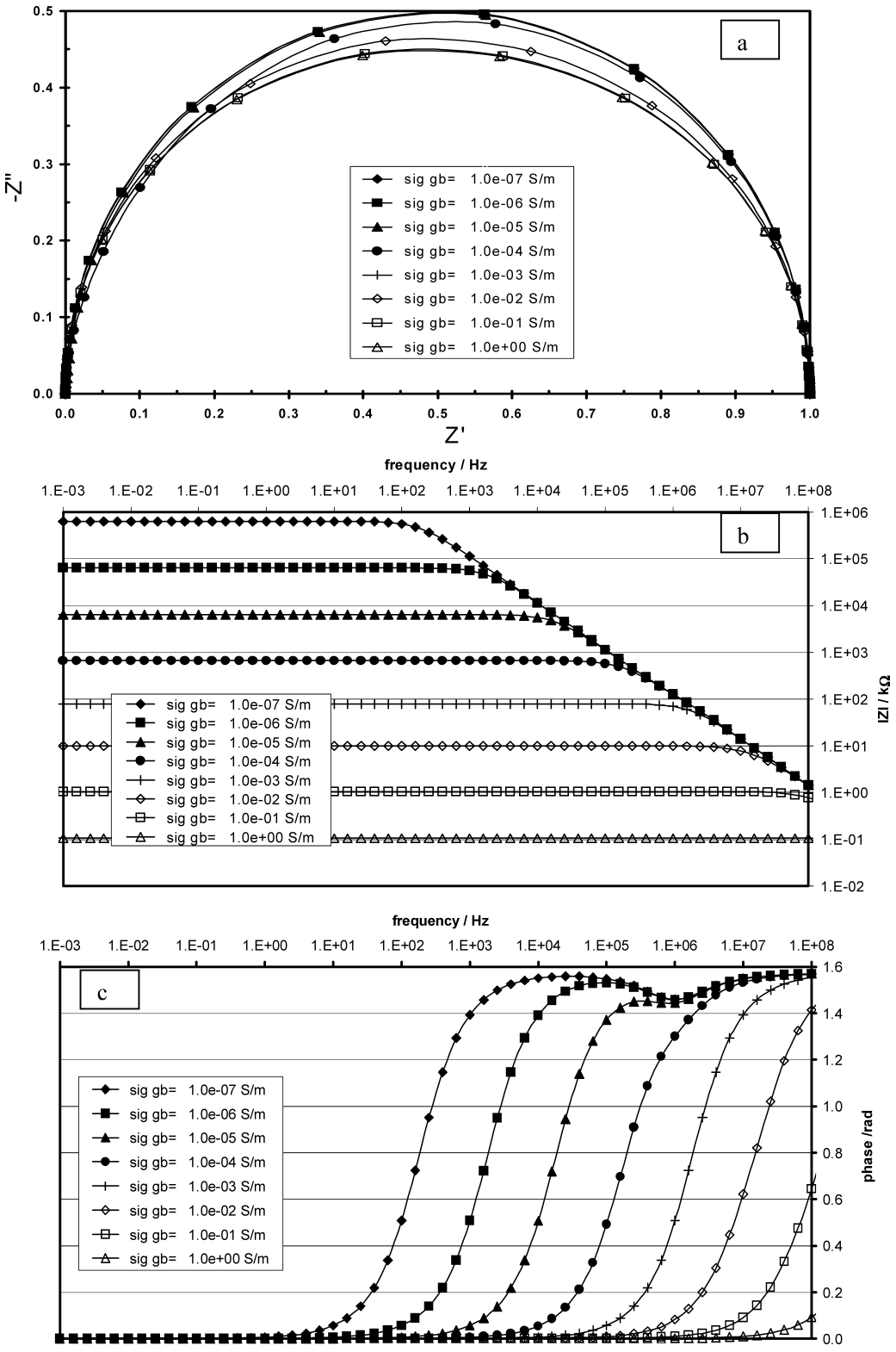

Fig. 6 Simulated impedance spectra using the BLM model for a cylindrical pellet with 4 mm diameter and 1 mm thickness. The mean grain size is taken as $D = 0.5$ nm. The grain conductivity is taken as $\sigma_g = 10^{-3}$ S/m and the gb conductivity is varied between 10^{-7} and 1 S/m. a) Complex plane plot, b) Bode modulus representation, c) Bode phase representation.

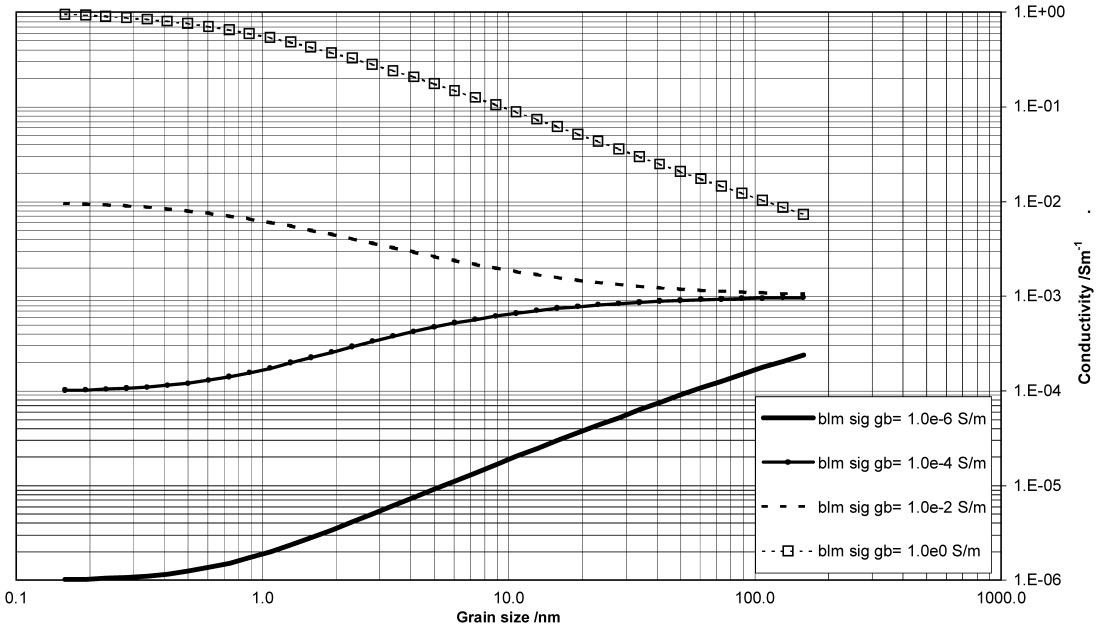

Fig. 7 Grain size dependence of the electrical conductivity of a cylindrical pellet with 4 mm diameter and 1 mm thickness using the BLM model for 4 gb conductivity values: 10^{-6}, 10^{-4}, 10^{-2} and 1 S/m.

very unfavorable gb/grain area, an important short-circuit of the grain resistance by the parallel path is only observed for the largest gb conductivity, 1 S/m (Fig. 3b and Fig. 7). Therefore, if only one relaxation time is visible, the diameter of the arc can be taken in first approximation as the grain resistance. The general conclusion is that parallel effects are usually small for large grain size and isotropic grain boundaries. The BLM can be used most often without major problems.

When the grain size decreases ($D = 50$ nm cf. Fig. 4, $D = 5$ nm cf. Fig. 5), the overall impedance is progressively dominated for low gb conductivity by the low frequency arc, corresponding to the blocking grain boundary (see Fig. 7). This reflects the progressive increase of the grain boundary volume fraction in the Bauerle model. At very small grain size, the parallel boundary effect appears for σ_{gb} of the same order as σ_g, i. e. for $D = 0.5$ nm and $\sigma_{gb} = 10^{-3}$ S/m, the diameter of the perfect semicircle (Fig. 6a) is equal to one half of the grain resistance. The Bode plots (Fig. 6b and c) show most clearly the influence of the grain boundary conductivity and of the parallel path for high σ_{gb} on sample impedance. Two relaxation frequencies are observed for $\sigma_{gb} > 10^{-4}$ S/m. In the Nyquist plot for 0.5 nm grain size (Fig. 6a), the impedance arcs appear slightly depressed for $\sigma_{gb} > 10^{-3}$ S/m. In this case, the classical BLM has no physical significance. Only a resolution of the analytical Eqs. (18–21) permits the calculation of individual electrical parameters of grain and gb. However, the recently published "composite" model [20, 21] shows that both the classical BLM and the generalized BLM become physically unrealistic for grain sizes less than approximately ten times the grain boundary thickness. This shows up as DC conductivities less than the Hashin-Shtrikman lower bound, which is physically impossible for a two-phase composite system. Even though the generalized BLM is an improvement over the classical BLM, it still requires current to remain in one path or the other (the grain core/capping grain boundary path vs. the parallel grain boundary path of Fig. 1) instead of being able to communicate between the two paths (as in the "real" situation). The generalized BLM can be up to 30% in error when grain size and grain boundary width become comparable.

Let us now summarize the general conclusions from this model.

1) A single perfect impedance arc is obviously observed when grain and gb conductivity are identical ($\sigma_{gb} = \sigma_g = 10^{-3}$ S/m), but also, in the isotropic case, when the grains are completely short-circuited by parallel grain boundaries ($\sigma_{gb} \gg \sigma_g$ leading to $R_{gb//} \ll (R_g + R_{gb\perp})$). In the last case, the resistance of series grain boundaries is completely negligible in front of grain resistance leading to a single relaxation time. These effects are most clearly observed in the Bode plots (Fig. 3–6b and c). Using Eq. (18), it is apparent that the low frequency real axis intercept of this arc equals the parallel gb resistance (Fig. 7), in total contradiction with the conventional assumption:

$$R_1 + R_2 \approx R_{gb//} \tag{22}$$

For all other cases, we observe two more or less overlapping semi-circles.

2) For low gb conductivity values ($\sigma_{gb} << 10^{-3}$ S/m), the parallel path is negligible:

$$Z_{gb//} >> (Z_g + Z_{gb\perp}) \tag{23}$$

Using Eq. (15), the impedance of the system is therefore of the classical form [8, 9, 19]:

$$Z = Z_g + Z_{gb\perp} \tag{24}$$

The characteristic relaxation frequencies are:

$$\omega_g >> \omega_{gb\perp} \tag{25}$$

The high frequency arc can be safely attributed to the grain interior and the low frequency arc to the series gb. The ratio of grain and gb resistance or capacitance is proportional to the grain size:

$$\frac{R_g}{R_{gb\perp}} = \frac{\sigma_{gb} D}{\sigma_g d} \tag{26}$$

$$\frac{C_g}{C_{gb}} = \frac{\varepsilon_g d}{\varepsilon_{gb} D} \tag{27}$$

These simple equations can give useful insight into the sample microstructure and specific electrical properties of grain and gb [18, 22].

4. Conclusions

The grain-size dependence of impedance spectra was discussed based on analytical equations obtained from the equivalent circuit of a microstructural 3D model of electroceramics, taking the parallel gb path explicitly into account. In this work, isotropic boundaries are considered: this corresponds physically for example to ionic conducting ceramics without precipitated gb phases or composite materials with core-shell structure. Comparing our previous work with anisotropic gb, a major difference of the isotropic gb model is that a single impedance arc can be observed for large gb conductivity values, i.e. when the series path (grain + series gb) is completely short-circuited by the parallel gb path.

Concerning the implications for experimental measurements on nanocrystalline ceramics and nanocomposites, impedance spectroscopy is an excellent tool for characterization of electrical properties of such materials. However, it needs a specific electrical model, based on a careful consideration of the microstructure. Furthermore, the experimentally accessible frequency domain is classically limited, from 10^7 to 10^{-4} s^{-1} in the best case. In Nyquist plots, we show that in most cases only one arc is apparent while the second is too small to be observed 1) at high frequency either when $\sigma_{gb} >> \sigma_b$ or for nanocrystalline ceramics with blocking gb 2) at low frequency in the microcrystalline case when σ_{gb} slightly above σ_b.

The measurement of grain properties in nanomaterials is thus not a trivial task. One should always compare with the same material as single crystal and in microcrystalline form.

References

1. J. Jamnik and J. Maier, *Solid State Ionics*, **94**, 189–198 (1997).
2. J. Maier, *Prog. Solid State Chem.*, **23**, 171 (1995).
3. P.A. Cox, *The Electronic Structure and Chemistry of Solids* (Oxford Science, Oxford, 1987).
4. A. Atkinson, *Solid State Ionics*, **28–30**, 1377 (1988).
5. M. Aoki, Y.-M. Chiang, I. Kosacki, L.J.R. Lee, H.L. Tuller, and Y. Liu, *J. Am. Ceram. Soc.*, **79**, 1169 (1996).
6. X. Guo and J. Maier, *J. Electrochem. Soc.*, **148**, E121 (2001).
7. A. Tschöpe, in *Solid State Ionics-2002*, edited by P. Knauth, J.-M. Tarascon, E. Traversa, and H.L. Tuller (Mat. Res. Soc. Symp. Proc., Vol. **756**, Warrendale, PA, 2003), p. 27.
8. J.B. Bauerle, *J. Phys. Chem. Solids*, **30**, 2657 (1969).
9. J.R. Macdonald, *Impedance Spectroscopy—Emphasizing Solid Materials and Systems* (J. Wiley, New York, 1987).
10. N.M. Beekmans and L. Heyne, *Electrochim. Acta.*, **21**, 303 (1976).
11. T. Van Dijk and A.J. Burggraaf, *Phys. Stat. Sol.* (*a*), **63**, 229 (1981).
12. M.J. Verkerk, B.J. Middelhuis, and A.J. Burggraaf, *Solid State Ionics*, **6**, 159 (1982).
13. J. Philibert, *Diffusion et transport de matière dans les solides*, Editions de Physique, Les Ulis, 1987, p. 227.
14. J. Fleig, *Solid State Ionics*, **131**, 117 (2000).
15. J. Fleig and J. Maier, *J. Electrochem. Soc.*, **145**, 2081 (1998).
16. J. Fleig and J. Maier, *J. Europ. Ceram. Soc.*, **19**, 696 (1999).
17. H. Näfe, *Solid State Ionics*, **13**, 255 (1984).
18. J.-H. Hwang, D.S. McLachlan, and T.O. Mason, *J. Electroceramics*, **3**, 7 (1999).
19. T.O. Mason, J.-H. Hwang, N. Mansourian-Hadavi, G.B. Gonzalez, B.J. Ingram, and Z.J. Homringhaus, in *Nanocrystalline Metals and Oxides: Selected Properties and Applications*, edited by P. Knauth and J. Schoonman (Kluwer Academic, Boston, 2002), p. 111.
20. N.J. Kidner, Z.J. Homrighaus, B.J. Ingram, T.O. Mason, and E.J. Garboczi, *J. Electroceramics*, **14**, 283 (2005).
21. N.J. Kidner, Z.J. Homrighaus, B.J. Ingram, T.O. Mason, and E.J. Garboczi, *J. Electroceramics*, **14**, 293 (2005).
22. C.M. Kleinlogel and L.J. Gauckler, *J. Electroceramics*, **5**, 231 (2000).
23. R. Bouchet, P. Knauth, and J.-M. Laugier, *J. Electrochem. Soc.*, **150**, E348 (2003).